Pressure-Induced Intermolecular Interactions in Crystalline Silane-Hydrogen

Wai-Leung Yim,[1] John S. Tse,[2,*] and Toshiaki Iitaka[3]

[1]*Institute of High Performance Computing, 1 Fusionopolis Way, No. 16-16 Connexis, Singapore 138632*
[2]*Department of Physics and Engineering Physics, University of Saskatchewan, Saskatoon, Canada, S7N 5E2*
[3]*Computational Astrophysics Laboratory, RIKEN, 2-1 Hirosawa, Wako, Saitama, Japan, 351-0198*

(Received 11 March 2010; revised manuscript received 6 August 2010; published 17 November 2010)

The structure and dynamics of a recently discovered solid silane-hydrogen complex under high pressure are elucidated with first-principles molecular dynamics calculations. A structure with orientationally disordered silane and hydrogen with their centers of mass arranged in a distinctive manner are found. Natural bond orbital analysis reveals that perturbative donor-acceptor interactions between the two molecular species are enhanced by pressure. The experimentally observed anticorrelated pressure-frequency dependency is a consequence of these novel interactions. Moreover, the experimentally observed multiple Raman peaks of H_2 can be explained by temporal changes in the environment due to deviations of the lattice parameters from the ideal cubic lattice.

DOI: 10.1103/PhysRevLett.105.215501 PACS numbers: 61.43.Bn, 62.50.−p, 63.20.dk

Many new structural types have been identified in the high pressure polymorphs of simple elemental solids [1]. These structures are often accompanied by novel electronic properties, such as superconductivity and metal-insulator transitions [2]. The effect of pressure on molecular compounds is equally fascinating. For example, silane (SiH_4) has been predicted [3,4] and observed [2] to be a superconductor at high pressure, although the mechanism is still controversial. Solid hydrogen (H_2) is arguably the most studied high pressure system [5]. Even for this seemingly simple molecule, features of the phase diagram are still not fully understood. Recently, a mixture with an approximate stoichiometry of $2H_2$:$1SiH_4$ was found to form a fcc crystal at about 6 GPa [6]. This crystalline molecular complex exhibits several peculiar properties. Within the pressure range 6–35 GPa, the observed frequencies of the H_2 vibrons are lower than in the solid phase at similar pressures [7]. Remarkably, several of the vibron modes were found to be anticorrelated with pressure, showing a monotonic decrease starting at ~6 GPa. Strobel *et al.* also observed a few modes that initially increased in frequency with increasing pressure, but these modes plateau and begin to decrease at pressures that are much lower than in pure H_2 [6]. The observed trends are opposite of those previously reported for H_2 dissolved in rare-gas matrices where the frequency increases monotonically with pressure [8]. Since both SiH_4 and H_2 are nonpolar closed-shell molecules, upon compression, one would anticipate nonbonded repulsions will dominate. The observed anticorrelation of H_2 frequency, however, suggests the presence of an unusually strong interaction between SiH_4 and H_2 that leads to weakening of the covalent bond at relatively low pressure. In this Letter, a crystal structure with H_2 molecules located at two different sites which possesses the vibrational behavior consistent with experiments is proposed. As will be shown below, the weakening of the H-H bond is due to perturbative donor-acceptor interactions between localized occupied and unoccupied antibonding orbitals of SiH_4 and H_2.

Since x-ray scattering intensities are dominated by Si, the $F\bar{4}3m$ symmetry proposed [6] is mainly derived from orientationally disordered SiH_4 molecules occupying the fcc sites. Formally, the space group symmetry would be reduced when H_2 molecules are also taken into account. Initially, 4 orientationally disordered SiH_4 were put in the fcc sites and 8 H_2 were inserted into the unit cell employing the *ab initio* random searching procedure [9]. No satisfactory structures were found after many trials. Since there are 8 equivalent octahedral cavities in a fcc crystal, it is not unreasonable to place the H_2 in these sites. After geometry optimization [10], 4 H_2 were found to migrate to the tetrahedral sites. The resulting structure, distorted slightly from fcc, is rhombohedral $R3m$ and shows aligned rows of $\ldots SiH_4 \ldots H_2$ (tetrahedral site, T) $\ldots H_2$ (octahedral site, O) $\ldots SiH_4 \ldots$ along the cubic [111] direction [Fig. 1(a)]. From the knowledge of the low pressure crystalline structures of SiH_4 [11] and H_2 [8], it is likely that both SiH_4 and H_2 are dynamically orientational disordered. To test this hypothesis, *ab initio* canonical ensemble molecular dynamics (MD) calculations were performed at 300 K [12,13]. The result at 5.8 GPa is illustrated in Fig. 1(b). Examination of the trajectories reveals the SiH_4 and H_2 motions are correlated in order to reduce internal stress. Full geometry optimization on structures selected randomly from the MD trajectories show small distortions from the cubic lattice. Importantly, centers of mass (c.m.) of both species remain at their respective symmetry sites and the Si framework remains to be $F\bar{4}3m$. The procedure was repeated at different lattice parameters within the experimental pressure range of 6–35 GPa. The calculated equation of state is compared with experiment [6] in Fig. 1(a) and the agreement is excellent. It is noteworthy that this result is not affected by the choice of exchange-correlation functionals. Apart from a small shift to lower pressure, the absolute

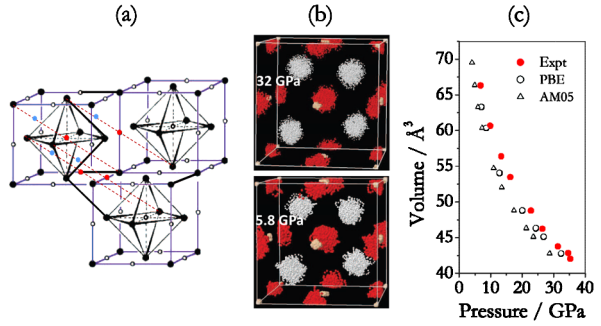

FIG. 1 (color online). (a) The proposed structure of the $4SiH_4 \cdot 8H_2$ showing the tetrahedral [filled light gray (blue) circles] and octahedral [filled dark gray (red) circles] sites occupied by H_2. The H_2 occupation sites aligned approximately along the body diagonal of the face-centered cubic lattice. (b) Temporal positions of SiH_4 and H_2 obtained from molecular dynamics calculations at 5.8 and 32 GPa. Hydrogen atoms of H_2 at the tetrahedral (white dots) and octahedral [gray (red) dots] sites are shown. (c) A comparison of the calculated (open circle, PBE; triangle, AM05) and experimental [filled gray (red) circles] equation of states for a crystalline solid of SiH_4 and H_2 in the stoichiometric ratio 2:1.

agreement between the Perdew-Burke-Ernzerhof (PBE) and Armiento-Mattsson (AM05) equation of states (the latter has shown to perform better for predicting lattice constants [14]) is very good with the PBE results closer to the experiment [Fig. 1(c)].

The vibrational frequencies for H_2 molecules were computed from Fourier transform of velocity autocorrelation functions in their center-of-mass frame from the MD trajectories at 300 K [12]. The calculated vibrational frequency for an isolated H_2 at 300 K of 4385 cm^{-1} is to be compared with the measured value of 4106 cm^{-1}. The vibrational density of states spans a range from 4150 to 4410 cm^{-1} [Fig. 2(a)]. Two groups of vibrational modes with different energies can be distinguished. In the higher energy group, the mean frequency increases slightly from 4391 cm^{-1} at 4.8 GPa to 4400 cm^{-1} at 20.1 GPa where it starts to decrease with

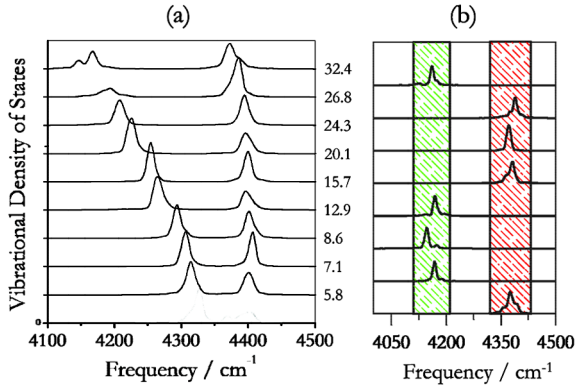

FIG. 2 (color online). (a) Calculated H_2 vibrational density of states at different pressures. (b) The frequency of individual H_2 vibron at 32.4 GPa. H_2 vibrons at the tetrahedral and octahedral sites are shaded in green (low frequency) and red (high frequency) rectangular boxes, respectively.

increasing pressure. In the lower energy group, the mean frequency decreases monotonically with increasing pressure. In the experiment [6], two vibrational bands were found to increase from about 4190 cm^{-1} at 6 GPa reaching a maximum of 4222 cm^{-1} at 28 GPa. On the other hand, frequencies of a group of 5 vibrational bands were observed to decrease with increasing pressure. The maximum span of the frequency between the first and second group is 170 cm^{-1}. This is to be compared with the calculated value of 250 cm^{-1}. The theoretical predictions reproduced the experimental trends, and the calculated frequencies are in semiquantitative agreement with

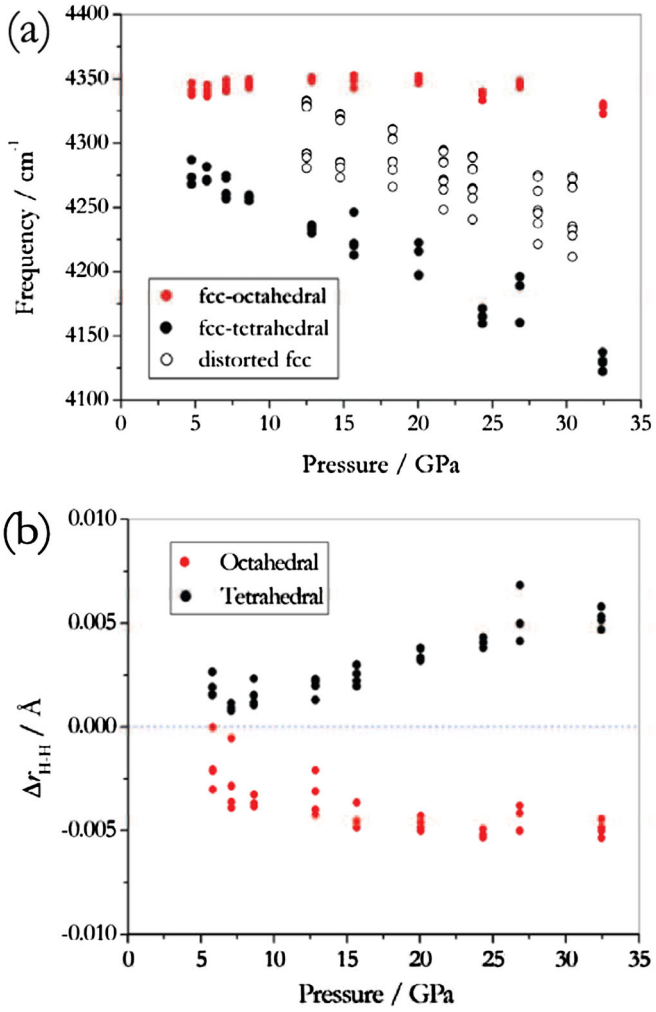

FIG. 3 (color online). (a) Plots of the H_2 vibrons for H_2 in the tetrahedral (filled black circles) and octahedral (filled red circles) sites of ideal fcc lattice as a function of pressure are shown. Frequency-pressure relationship of H_2 vibrons due to H_2 in distorted fcc lattice is also displayed (open circles). The four highest and the four lowest energy vibrations for the distorted structures are assigned to H_2 at the octahedral sites and tetrahedral sites, respectively. Vibrational frequency calculations in optimized (ideal or distorted fcc) structures were performed using the direct force constant approach. (b) Pressure dependence of the deviation of the H-H bond distance from a free H_2 molecule for H_2 in the tetrahedral (filled black circles) and octahedral (filled red circles) sites.

measured Raman spectra [Fig. 3(a)]. The two groups of vibrational modes are identified as H_2 vibrons located at the T and O sites, as demonstrated from the individual contributions at 32.4 GPa shown in Fig. 2(b), with vibron frequencies at the T sites lower than those at the O sites. It is also noted even within the respective sites that there are small differences in the frequencies.

From a geometric point of view, the c.m. of the H_2 in the T site is closer to a SiH_4 than in the O site. For a fcc crystal of unit cell size a, the closest distance from the T site to a corner atom is $\sqrt{3}/4a$, which is shorter than the distance from the O site to a face-centered atom of $\frac{1}{2}a$. Therefore, the H_2 bond in the T site is expected to be more perturbed than at the O site. This expectation is confirmed by the calculated H_2 bond lengths as a function of pressure shown in Fig. 3(b). The calculated H_2 bond lengths in compressed SiH_4-$2H_2$ deviate from that of the isolated H_2 (0.751 Å) molecule. Two distinct trends are observed. In the O sites, the H_2 bond lengths are shortened slightly with pressure and remain relatively constant at pressures above 24 GPa. In contrast, the H_2 bonds at the T sites increase almost linearly with increasing pressure by about 0.006 Å (0.756 Å) from the free molecular value at 32.4 GPa. The pressure dependences of the H_2 bond length in both sites are in accord with observed trends in the vibrational frequencies.

The H_2 vibrons are sensitive to the relative orientation to the nearest SiH_4. In the fixed cubic symmetry small stress anisotropy was found. Removing this constraint, the cubic cells are distorted slightly, but the H_2 are still in the T and O sites. The H_2 vibrons at the optimized distorted structures calculated from the direct force constant method are shown in Fig. 3(a) (open circles). The H_2 frequencies now spread between the two bands of frequencies computed from the cubic lattice. Small cell distortion is confirmed by variable cell MD calculations at 32 GPa (supplementary material [15]). The three axes of the rhombohedral cell are practically equivalent at 5.5 Å with a mean cell angle of 86°. The calculated bandwidth of the H_2 vibrons of 300 cm^{-1} (4000–4300 cm^{-1}) is comparable with the experimental width of 240 cm^{-1}. Extra peaks can now be identified from the calculated vibrational density of states. Therefore, the observed multiple Raman bands [6] can be attributed to temporal distortion from the ideal cubic unit cell.

Since SiH_4 and H_2 are closed-shell nonpolar molecules, when compressed, intermolecular interactions would involve localized electron pairs of the filled orbitals (donor) from one species to the unoccupied orbitals (acceptor) of the other. To investigate the electronic origin underlying the intuitive description (see below) in the crystalline environment, natural bond orbital (NBO) analysis [16–18] was performed on SiH_4-H_2 dimer model systems. In the NBO analysis, wave functions of the subsystem are transformed into localized forms followed by a perturbative calculation of the nonbonded interaction. The total energy can be decomposed into covalent and noncovalent components. The stabilization energy ($E^{(2)}$) attributed to the noncovalent (donor-acceptor) interaction is evaluated from second order perturbation theory [13], $E^{(2)} = -2\frac{\langle\psi_d|\hat{F}|\psi_a\rangle}{\varepsilon_a - \varepsilon_d}$, where $\hat{F}$ is the effective orbital Hamiltonian and ε_d and ε_a are the NBO energy for the donor and acceptor orbital, respectively, and ψ_d and ψ_a are the associated NBO orbital wave functions.

Examination of MD trajectories at several pressures revealed two distinctive configurations for H_2 located in the O and the T sites. H_2 at the O sites rotate about the line joining the c.m. and the Si atom bisecting the SiH_4 molecule [Fig. 4(a)]. At the T sites, the H_2 prefers to locate in the "pocket" formed from three Si-H bonds [Fig. 4(c)]. Since the H_2 rotates about its c.m., the vibrational frequencies and the second order noncovalent energy lowering $E^{(2)}$ were computed [18] at two positions representing the two extreme conformations—head-on and side-on—at the O and T sites (Fig. 4). For each Si to H_2 c.m. distance the structure of the SiH_4-H_2 complex is optimized. Representative results of the calculations are presented in Fig. 4.

The SiH_4-H_2 interactions at the O site will be discussed first. In Fig. 4(a), the vibrational frequencies and stabilization energy are shown as a function of the Si . . . H_2(c.m.) distance. When the H_2 approaches SiH_4 in the C_2 configuration, the frequency of the vibron in the side-on geometry increases initially and then decreases when the distance is shorter than 2.3 Å. For the head-on geometry, the vibron frequency decreases very slightly until the H_2 . . . SiH_4 c.m. distance is less than 4.0 Å. In the crystalline state, the distances between the c.m. of H_2 and SiH_4 vary from

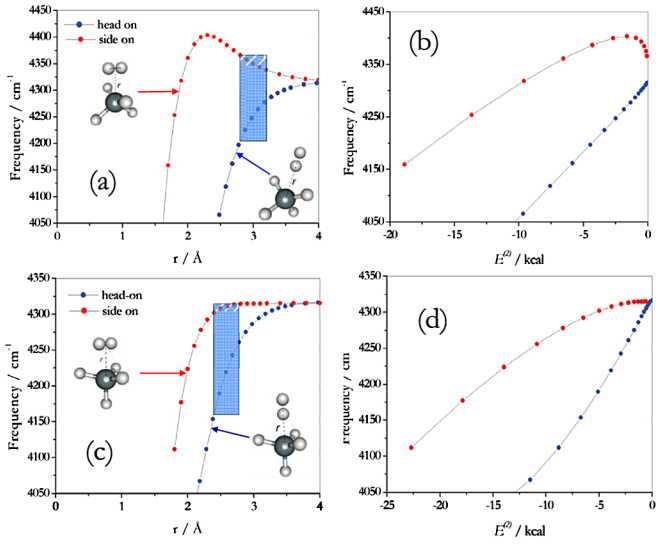

FIG. 4 (color online). (a) Plots of H_2 vibrational frequency as a function of the center-of-mass distance between SiH_4 and H_2 molecules in the head-on (filled blue circles) and side-on (filled red circles) configurations along the C_2 symmetry axis; the separation range distance relevant to the experimental pressure range is shaded in a blue rectangular box. (b) The dependence of vibrational frequency on the $E^{(2)}$ energy for H_2 approaching SiH_4 along C_2 symmetry axis is plotted. (c),(d) Similar analyses as done in (a) and (b) for SiH_4-H_2 approaching each other along the C_3 symmetry axis of SiH_4 are shown.

3.2 Å at 5.8 GPa to 2.8 Å at 32.4 GPa. The frequency range relevant to this separation is shaded in Fig. 4(a). The H_2 vibron frequency decreases from 4279 cm^{-1} at 5.8 GPa to 4205 cm^{-1} at 32.4 GPa. In comparison, the frequency of the vibron for the side-on geometry within this distance range changes from 4338 cm^{-1} to 4366 cm^{-1}, an increase of 28 cm^{-1}. Note that when a H_2 lies at the edge of the fcc cell pointing toward two SiH_4 molecules, i.e., head-on orientation, this molecule is also orientated in the side-on configuration relative to the other four SiH_4 groups forming the octahedral site. The shift of the vibron frequency is estimated to be -36 cm^{-1} from this simple model, while the corresponding shift in the vibron frequency calculation from MD is about -13 cm^{-1} [Fig. 2(a)]. Between 2.8 and 3.2 Å, the calculated stabilization energy $E^{(2)}$ due to noncovalent interaction for the side-on geometry is negligibly small, but for the head-on geometry, the energy is lowered by -1.5 to -4.4 kcal/mol [Fig. 4(b)].

In the head-on interaction along the C_2 symmetry axis, the NBO orbital energies show the strongest interaction is the charge-transfer from occupied σ bond of Si-H (σ_{SiH}, donor) to the lowest unoccupied H-H antibonding (σ^*_{HH}, acceptor) orbital. For other configurations, charge transfer from σ_{HH} to $\sigma^*_{Si\text{-}H}$ is predominant. A similar analysis was also performed on the C_3 configuration at the T site. For this site, the distance between H_2 and SiH_4 is 2.78 Å at 5.8 GPa and 2.40 Å at 32.4 GPa. Within the relevant separation, the head-on interaction led to a decrease of H_2 vibrational frequency from 4261 cm^{-1} to 4161 cm^{-1}, a decrease of 100 cm^{-1}. The corresponding stabilization energy is about -4 kcal/mol. There are no appreciable changes in the vibron in the side-on geometry. Therefore, the simple dimer models reproduce semiquantitatively the essential features observed by experiment and predicted from MD calculations.

Static and dynamic calculations show the stoichiometric SiH_4:$2H_2$ crystal at high pressure has a structure with 4 SiH_4 in the fcc sites and 8 H_2 equally split between the T and O sites and aligned along the [111] directions. SiH_4 and H_2 are fluxional and orientationally disordered. The observed frequency-pressure anticorrelation was reproduced. The H-H vibrons are found to be sensitive to the local environment with H_2 in the T sites more perturbed by the surrounding than at the O site. The observed multiple Raman peaks are due to temporal deviation from the fcc lattice. NBO analysis shows that donor-acceptor interactions are enhanced by the shortening of the SiH_4-H_2 separation under pressure and contribute to the stability. The exploitation of the second order intermolecular interaction between closed-shell molecules may lead to the synthesis of new classes of otherwise inaccessible H_2-bearing molecular systems [19].

The authors thank an anonymous referee for pointing out an incorrect identification of the lower symmetry subgroup in an earlier version of this Letter. This led to the correct result now presented in this Letter. This work was partially supported by KAKENHI (No. 20103005 and No. 19310083) from MEXT.

*To whom correspondence should be addressed.
John.tse@usask.ca

[1] J. S. Tse, Z. Kristallogr. **220**, 521 (2005).
[2] M. I. Eremets *et al.*, Science **319**, 1506 (2008); Y. Yao, J. S. Tse, and D. D. Klug, Phys. Rev. Lett. **102**, 115503 (2009); Y. Ma *et al.*, Nature (London) **458**, 182 (2009); T. Matsuoka and K. Shimizu, Nature (London) **458**, 186 (2009).
[3] N. W. Ashcroft, Phys. Rev. Lett. **92**, 187002 (2004).
[4] Y. Yao, J. S. Tse, Y. Ma, and K. Tanaka, Europhys. Lett. **78**, 37 003 (2007).
[5] P. Tolédano, H. Katzke, A. F. Goncharov, and R. J. Hemley, Phys. Rev. Lett. **103**, 105301 (2009), and reference therein.
[6] T. A. Strobel, M. Somayazulu, and R. J. Hemley, Phys. Rev. Lett. **103**, 065701 (2009).
[7] R. J. Hemley, Annu. Rev. Phys. Chem. **51**, 763 (2000); F. Datchi *et al.*, Bull. Am. Phys. Soc. **41**, 564 (1996).
[8] H. K. Mao and R. J. Hemley, Rev. Mod. Phys. **66**, 671 (1994).
[9] C. J. Pickard and R. J. Needs, Phys. Rev. Lett. **97**, 045504 (2006).
[10] Calculations were performed using the VASP 4.6 package [G. Kresse and J. Hafner, Phys. Rev. B **47**, 558 (1993); G. Kresse and J. Furthmüller, Phys. Rev. B **54**, 11169 (1996)] employing projector plane wave (PAW) potentials [G. Kresse and J. Joubert, Phys. Rev. B **59**, 1758 (1999)]. PAW potentials were taken from the PBE functional [J. P. Perdew, K. Burke, and M. Ernzerhof, Phys. Rev. Lett. **77**, 3865 (1996)] pseudopotential library provided with the code. Convergence of the total energy with respect to the cutoff energies was examined. Plane wave and charge density cutoffs of 600 and 800 eV, respectively, were sufficiently high and were used in the calculations of the static structures. A $4 \times 4 \times 4$ k point set was used.
[11] O. Degtyareva *et al.*, Phys. Rev. B **76**, 064123 (2007).
[12] M. P. Allen and D. J. Tildesley, *Molecular Simulation of Liquids* (Oxford University Press, New York, 1988).
[13] The system was first scaled to 300 K in 0.5 ps. This is followed by equilibration for 1 ps. Then a molecular dynamics trajectory of 5 ps using Nosé thermostat [S. Nosé, J. Chem. Phys. **81**, 511 (1984); Mol. Phys. **52**, 255 (1984)] was collected. Time step was set to 1 fs. Plane wave and charge density cutoff energies were set to 250 and 400 eV, respectively. A $4 \times 4 \times 4$ k point set was used.
[14] R. Armiento and A. E. Mattsson, Phys. Rev. B **72**, 085108 (2005); A. E. Mattsson and R. Armiento, Phys. Rev. B **79**, 155101 (2009).
[15] See supplementary material at http://link.aps.org/supplemental/10.1103/PhysRevLett.105.215501 for detailed information pertinent to convergence test of energy cutoffs, detailed bonding interaction analysis, and rationales of vibron splittings.
[16] A. E. Reed, L. A. Curtiss, and F. Weinhold, Chem. Rev. **88**, 899 (1988).
[17] F. Weinhold and C. Landis, *Valency and Bonding: A Natural Bond Orbital Donor-Acceptor Perspective* (Cambridge University Press, Cambridge, England, 2005).
[18] Calculations were performed using GAUSSIAN 03, revision C.02 (M. J. Frisch *et al.*, Gaussian, Inc., Wallingford, CT, 2004) with the 6-311 + $G(2d, p)$ basis sets employing the PBE functional.
[19] N. W. Ashcroft, Physics **2**, 65 (2009).